The Theoretical Basis for the Parameterization of Ice Crystal Habits: Growth by Vapor Deposition

JEN-PING CHEN* AND DENNIS LAMB

Department of Meteorology, The Pennsylvania State University, University Park, Pennsylvania

(Manuscript received 8 April 1993, in final form 17 September 1993)

ABSTRACT

A theoretical analysis of surface kinetic and gas-phase diffusional effects permits the growth rates and habits of ice crystals to be specified in a self-consistent way. The analysis makes use of the fact that the difference between the condensation coefficients of the prism and basal faces determines the primary crystal habits, whereas the spatial variations of the vapor density contribute to the secondary habits. The parameterization scheme that results from the theoretical analysis yields a power law relationship between the a and c axial lengths that matches earlier empirical formulas derived from observational data for the temperature range of $-30°$ to 0°C. Through application of this adaptive parameterization in a microphysical model that categorizes ice particles according to both their masses and shapes, it is shown that deviations from the power law relationship may develop if the crystals experience significant variations in the air temperature and in their inherent growth habits. A mass–dimension relationship is also derived through the theoretical analysis that can be used as a less detailed parameterization scheme for the growth of ice crystals by vapor deposition.

1. Introduction

The formation of atmospheric ice crystals is frequently considered important to the initiation of precipitation, especially in midlatitude clouds. In recent years, increasing attention has also been paid to high cirrus clouds, composed almost exclusively of ice crystals, because of their important roles in the global radiation budget (Stephens et al. 1990; Wielicki et al. 1990). In contrast to liquid-phase cloud particles, ice crystals play far more complicated roles in the microphysical and radiative transfer processes of clouds. Much of the complexity stems from the fact that ice crystals exist in a wide variety of shapes. For instance, the fall speeds of ice crystals of similar mass can differ considerably depending on their specific shapes (Locattelli and Hobbs 1974; Fukuta 1980). The shapes of the ice particles also affect the cloud radiation budget through their impact on the scattering phase function (Stephens et al. 1990). Despite the importance of ice in the atmosphere, our present knowledge on how the sizes and shapes of ice crystals evolve in clouds is quite limited.

The shapes of ice crystals, often referred to as the growth habits, exhibit very strong dependences on temperature and, to a lesser degree, on supersaturation (Nakaya 1954; Hallet and Mason 1958; Kobayashi 1961). Many workers have noted the transitions of the primary habits from plate to column (~ −4°C), back to plate (~ −9°C), and then to column again (~ −22°C) as the temperature decreases (Kobayashi 1961; Hallett and Mason 1958; Fukuta 1969; Ryan et al. 1976). This remarkable temperature dependence of the primary growth habits gives evidence for the fundamental difference of the linear growth rates of individual basal and prism faces (Lamb and Hobbs 1971). The secondary habits are modifications to the primary forms that appear when the crystals grow in regions of high supersaturations. Such modifications may appear simply as exaggerations of the prevalent primary habits, as when needles develop from columns, or as distinct changes in shape, as when dendrites evolve from simple planar crystals. The secondary habits result from the nonlinear interactions that exist between the crystal shape and the distribution of water vapor in the immediate vicinity of the crystal.

Many observational studies (e.g., Ono 1969, 1970; Auer and Veal 1970) have attempted to quantify the crystal growth rates and thus provide an empirical basis for developing parameterizations of the crystal shapes that could be applied in numerical cloud models. However, such strictly observational approaches usually lack physical interpretation. As a result, many of the parameterization schemes used previously for the simulation of ice crystal shapes are often oversimplified

* Also affiliated with the Center for Clouds, Chemistry, and Climate, Scripps Institution of Oceanography, University of California, San Diego, La Jolla, California.

Corresponding author address: Dr. Jen-Ping Chen, Center for Clouds, Chemistry, and Climate, Scripps Institution of Oceanography, University of California, La Jolla, CA 92093-0239.

and incapable of allowing for habit modification as the crystals enter different growth regimes. In this paper, we discuss some of the earlier parameterizations and their deficiencies. Then, through a theoretical approach, we offer a physical explanation for a commonly used habit parameterization. A simple but rigorous procedure is then developed that allows for changes in the shapes of the ice crystals during depositional growth over a wide range of conditions. Finally, this scheme is applied in a detailed microphysical model to simulate the evolution of the size and shape distribution of ice crystals in a representative cloud.

2. Previous studies of ice growth habits

a. Measurements and observations

Ice crystal growth habits have been studied in the past using a variety of techniques, some employed in the field and some in the laboratory. The overall purpose of the early studies was to demonstrate reproducible relationships between the observed habits and the environmental conditions at the time of growth. Nordenskiöld (1893) may have been the first observer to recognize that vapor-grown ice crystals can be broadly classified into columnar and platelike forms, but it was not until the systematic laboratory investigations of Nakaya and Sakido (1936) that a reproducible connection could be made between the observed forms and the growth temperature and ambient humidity. Later field observations (e.g., Weickmann 1949; Magono and Lee 1966) and laboratory studies (e.g., aufm Kampe et al. 1951; Mason 1953; Hallett and Mason 1958; Kobayashi 1961; Fukuta 1969) served to confirm and refine our knowledge of the dependence of ice crystal habits on temperature and supersaturation.

The primary habit of an ice crystal that results from growth under a specific set of environmental conditions is determined by the relative growth along the main crystallographic directions. Direct measurements of the linear growth rates of individual prism and basal faces of ice grown on a substrate were made as functions of temperature (−17° to −2.5°C), excess vapor density, and partial pressure of air by Lamb and Scott (1972). They measured the linear growth rates in a pure water vapor environment to eliminate the effect of air on the transport of water vapor to the crystal surfaces. Lamb and Scott (1972, 1974) attributed the variation of the growth rates with temperature to the peculiar trends in the condensation coefficients and the effect of crystal surface kinetics. Sei and Gonda (1989) measured the condensation coefficients at several temperatures between −30° and 0°C and adopted the so-called vapor/liquid/solid growth mechanism proposed by Kuroda and Lacmann (1982) to interpret the habits of ice crystals growing at temperatures near the melting point. These types of laboratory measurements showed that temperature is the controlling factor of the primary growth habits. Although these experimental results are not sufficient to fully describe the growth and the secondary habits of ice crystals in real clouds, they are valuable to the theoretical discussions presented in the next section.

While the primary habits are strongly correlated with temperature, the secondary habits are controlled by more complicated factors. In their laboratory measurements of ice crystals growing in air, Shaw and Mason (1955) were able to give an approximate description of the growth of the individual faces:

$$(2a)^2 = U_a t + A, \tag{1}$$

$$(2c)^2 = U_c t + B, \tag{2}$$

where a and c are, respectively, the a and c axis lengths; U_a, U_c, A, and B are constants; and t is the time of growth. Todd (1965) measured the lengths of the a and c axes of crystals sampled in cumulus clouds and found deviations from the above $t^{1/2}$ law. He proposed that U_a, U_c, and the exponent of the power law should be temperature dependent. Ono (1969, 1970), Auer and Veal (1970), Heymsfield and Knollenberg (1972), Davis (1974), as well as Jayaweera and Ohtake (1974), measured the dimensions of naturally occurring ice crystals and found an exponential relationship between the two axes of the following form:

$$c = \eta a^{\beta}, \tag{3}$$

where η and β are positive constants that have specific values corresponding to the particular crystal types. However, no physical explanations have been provided for such a power law relationship.

b. Numerical simulations and parameterizations

Earlier ice-phase microphysical models, especially those adopting bulk water parameterizations, tend to ignore the habits of ice crystals. Recognizing the importance of crystal habits to various growth processes of ice particles, Cotton (1972) divided the crystal habits into seven temperature regimes. For each regime, the aspect ratio of ice crystals was assumed constant throughout the growth. Hall and Pruppacher (1976) adopted the exponential relationship (3) to describe the characteristic dimensions of the a and c axes. Yet, since only one set of the coefficients η and β was assigned to represent columnar ice and another set for planar ice, their results overlooked the temperature dependence of the secondary habits. Miller and Young (1979) suggested the existence of three principal stages of ice crystal growth from the vapor: 1) isometric growth, 2) constant axial ratio growth, and 3) limiting dimension growth. According to this scheme, very small ice crystals (<3 μm) grow nearly isometrically, that is, uniaxially. The crystals then enter a stage where they attain a characteristic axis ratio. Large crystals grow mainly along the major axis and the dimension of the minor

axis is limited. Miller and Young assumed that the minor axis will cease to grow after reaching a *limiting dimension.* The constant axial ratio and the *limiting dimension* are both temperature dependent and, therefore, reflect the secondary habits to some extent. However, the artificial division of the growth into separate stages emulates discrete processes that do not exist in nature. Also, neither the temperature-dependent surface kinetic nor the gas-phase transport effects can be properly described with such a scheme.

Hindman and Johnson (1972) applied the expression developed by Todd (1965) for the growth along the a and c axes at a constant temperature in a water saturated environment:

$$a = K_a t^A,$$
$$c = K_c t^B, \tag{4}$$

where K_a, K_c, A, and B are parameters that depend only on the temperature. Note that these two formulas can be combined to give

$$c = \frac{K_c}{K_a^{B/A}} a^{B/A}, \tag{5}$$

which is the same as (3) when $\eta = K_c/K_a^{B/A}$ and $\beta = B/A$. This application of expression (3) represents an improvement in that both η and β can be temperature dependent. The values of β they used do reflect the transitions of the primary habits near $-4°$, $-9°$, and $-20°$C except that β is set to unity at temperatures above $-4°$ and below $-20°$C. Equation (5) provides a better parameterization for the habits than does the simple empirical representation (3) because of the inclusion of the temperature-dependent coefficients β, despite the fact that the values they used for A and B are oversimplified. The above formulas are derived according to observational data, but the physics behind them remains unexplained. In the following discussion, a more physically based theoretical explanation will be provided for the parameterization of the growth habits.

3. Theoretical basis for the parameterization of the growth habits

a. *Effects of surface kinetics*

The rate at which water molecules deposit onto the face of an ice crystal and contribute to its growth is directly proportional to the kinetic theory impingement flux and the probability that an impinging molecule is able to build into the condensed phase (Burton et al. 1951; Rooth 1967; Pruppacher and Klett 1978, pp. 133, 415). This probability is in effect a parameter, the "condensation coefficient" (α), that empirically accounts for the various kinetic (rate) processes responsible for incorporation of molecules into the crystal lattice (Lamb and Scott 1974; Kuroda 1982; Kuroda and Lacmann 1982). Note that, as used here, α is more than a "sticking coefficient," the probability that an impinging vapor molecule becomes adsorbed in the first place, as it also accounts for adsorbed molecules that subsequently evaporate before becoming a part of the crystal lattice (Lamb and Scott 1974). It is beyond the scope of this paper to discuss the theoretical basis for variations of α with temperature or with the local supersaturation. Here, we simply accept the functional forms of the condensation coefficients as given by past experimental data and as discussed later in this section.

Mathematically, the molecular flux into the crystal lattice across a particular low-index face, here either the basal (0001) or prism ($10\bar{1}0$) face, is given by the net condensation flux (Pruppacher and Klett 1978, p. 133)

$$J = \frac{\alpha}{4} \bar{\nu} \delta\rho, \tag{6}$$

where $\bar{\nu}$ is the mean molecular speed and $\delta\rho = \rho_j - \rho_s$ is the local or "interfacial" excess vapor density, the difference between the vapor density at a "vapor jump" distance (Pruppacher and Klett 1978, p. 414) from the crystal surface, ρ_j, and the equilibrium value, ρ_s, which is a characteristic of the surface. The interfacial vapor density ρ_j in contact with the solid cannot be measured in the presence of a noncondensing gas (e.g., air) since significant vapor gradients are set up in the vicinity of any growing or evaporating particle (Rooth 1957; Fuchs 1959, p. 7).

Some estimate of the magnitude of ρ_j and therefore $\delta\rho$ can be gained by assuming that the distribution of vapor about the crystal is stationary (time invariant) and then matching the boundary conditions between the kinetic theory expression for the condensation flux and the continuum specification for the diffusive flux of water vapor toward the crystal interface from the gas phase surrounding the particle. This approach is conventionally used to calculate the growth of water drops in air (Rooth 1957; Fuchs 1959, p. 7; Pruppacher and Klett 1978, p. 415), in which case the calculation is relatively precise by virtue of the simplifying assumptions made possible by the spherical symmetry of the problem. For a spherical particle of radius r the interfacial vapor density is found to be

$$\rho_j = \frac{\rho_\infty + \dfrac{\alpha\bar{\nu}}{4D_v} r\rho_s}{1 + \dfrac{\alpha\bar{\nu}}{4D_v} r}, \tag{7}$$

where ρ_∞ is the ambient vapor density far removed from the particle, and D_v is the vapor diffusivity. The interfacial excess vapor density driving the growth of the spherical particle is therefore

$$\delta\rho = (\rho_\infty - \rho_s) \Big/ \left(1 + \frac{\alpha\bar{\nu}}{4} \frac{r}{D_v}\right), \tag{8}$$

so the net condensation flux is

$$J = \frac{\alpha\bar{\nu}}{4}(\rho_\infty - \rho_s)\Big/\left(1 + \frac{\alpha\bar{\nu}}{4}\frac{r}{D_v}\right). \quad (9)$$

Note that in the common case in which the diffusion speed D_v/r is much less than the effective molecular speed $\alpha\bar{\nu}/4$,

$$J \approx \frac{D_v}{r}(\rho_\infty - \rho_s). \quad (10)$$

This result shows that the condensation flux to a spherical particle growing in a diffusion-limited regime is insensitive to the magnitude of the condensation coefficient.

In the case of a nonspherical particle bounded by flat faces that may have distinctly different condensation coefficients, as with hexagonal ice crystals, we must consider spatial dimensions other than the radial coordinate. Indeed, as the one-dimensional drop-growth problem shows, the condensation flux (and thus the linear growth rate of the interface) may not be a sensitive function of the condensation coefficient. Nevertheless, real ice crystals do grow into complicated forms at least in part because the condensation coefficient of the basal faces (α_c) and the condensation coefficient of the prism faces (α_a) have different dependences on temperature (Lamb and Scott 1974). The habits of ice crystals growing in air can be understood only through a consideration of the interactions that take place between the surface kinetic processes and the multidimensional distribution of vapor about the crystal (Mason 1993).

At this time, we can at best provide an approximation to the solution of the complicated problem posed by the growth of hexagonal crystals in a relatively dense gaseous medium. The one-dimensional analysis teaches us that, even in the diffusion-limited case, the interfacial excess vapor density over a surface, $\delta\rho$, is very sensitive to the surface rate processes. This sensitivity can be seen by considering the expression for $\delta\rho$ when $D_v/r \ll \alpha\bar{\nu}/4$. Then,

$$\delta\rho \approx \frac{4D_v}{\alpha\bar{\nu}r}(\rho_\infty - \rho_s) \propto \frac{1}{\alpha} \quad (11)$$

when other factors are fixed. Thus, as the condensation coefficient of a face varies, so will the local excess density of vapor over that face, but in an opposing sense. This direct influence of the surface kinetics on the local vapor density, analogous to the change in voltage drop across a variable resistor in a constant-current electrical circuit, provides the mechanism by which the face-to-face variations of condensation coefficients cause the primary habits of a crystal to be realized even when the crystal as a whole is growing in a diffusion-limited regime. Consider, for instance, two adjacent faces, one basal and the other prism, characterized by different values of α. The local excess vapor density over each face will therefore be distinct, leading to the formation of a relatively strong *lateral* gradient of vapor density near the edge bounding the two faces of the crystal. This gradient in chemical potential, in turn, drives a lateral diffusive flux of vapor molecules that simultaneously takes vapor from the interface with the smaller value of α and donates it to the interface with the larger α. Vapor initially diffusing radially toward the crystal from afar in effect becomes "focused" in the vicinity of the crystal toward the most rapidly growing faces.

The net effect of this lateral redistribution of vapor on the relative growths of adjacent basal and prism faces is quantitatively difficult to determine, but the sense of the redistribution is clear. Here, we propose a tentative "mass distribution hypothesis" that takes the multidimensionality of the physical problem into account and operates in the correct sense:

$$\frac{dc}{da} = \frac{\alpha_c(T)}{\alpha_a(T)}\frac{\nabla\rho_c}{\nabla\rho_a} \equiv \Gamma(T)\Phi(c, a). \quad (12)$$

Here, dc/da is the ratio of the linear growth rates along the c and a directions, while

$$\Gamma(T) \equiv \frac{\alpha_c(T)}{\alpha_a(T)} \quad (13)$$

is the ratio of the condensation coefficient for the basal face (subscript c) and that for the prism face (subscript a), whereas

$$\Phi(c, a) \equiv \frac{\nabla\rho_c}{\nabla\rho_a} \quad (14)$$

is the ratio of the macroscopic gradients of vapor density along the c and a axes, respectively. We call the ratio of the two condensation coefficients, Γ, the *inherent growth ratio* or *habit*. This important parameter is primarily a function of temperature and is driven by surface kinetic processes. The parameter Φ is a function of the dimensions a and c of the ice crystals and accounts for the nonspherical shape of the crystal. This function, as will be shown in the next section, can be derived by solving the Laplace equation for diffusion problems. The mass distribution law used here in effect suggests that the net flux of vapor toward a particular crystallographic face is reduced as the probability of molecular incorporation into that face is reduced. Physically, however, it is more likely that the lateral diffusive fluxes partially cancel any nonradial gradients in vapor density near the crystal edges and make the magnitude of $\delta\rho$ more or less uniform about the crystal.

b. Effects of crystal shape

As with the distorted electrostatic fields surrounding a nonspherical conductor, the radial gradient of vapor surrounding the ice crystal is greatest where

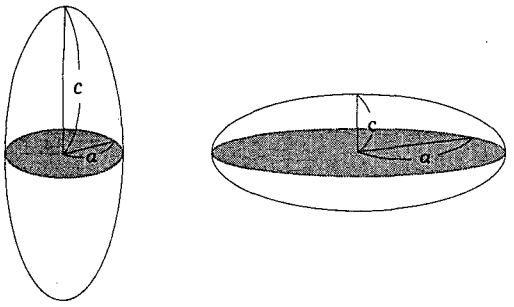

FIG. 1. Perspective views of prolate and oblate spheroids that resemble columnar and planar ice crystals, respectively.

the surface curvature is largest. The analogy between the field of vapor density ρ around a cloud particle and the field of the electrostatic potential around a charged conductor was shown to exist as early as the late nineteenth century by Stefan (1873) and Maxwell (1878) during studies of the condensation/evaporation process in relation to observed wet-bulb temperatures. Jeffreys (1918) also introduced the solution of the steady-state diffusion equation, which was later applied to the growth of droplets by Houghton (1950). As with the *electrostatic analogy, Fick's first law* of diffusion can be used to establish the vapor flux

$$\mathbf{J} = -D_v \nabla \rho, \tag{15}$$

where D_v is the diffusivity of water vapor in air and ρ is the local vapor density. Applying the continuity equation for ρ, with the assumption of incompressible airflow, we have *Fick's second law* (or the *diffusion equation*):

$$\frac{\partial \rho}{\partial t} = -\nabla \cdot \mathbf{J} = D_v \nabla^2 \rho, \tag{16}$$

where D_v is assumed to be independent of position. Since the characteristic time for vapor diffusion to a drop of radius r (Hidy and Brock 1970, p. 102),

$$\tau_{\text{dif}} = \frac{r^2}{\pi D_v}, \tag{17}$$

is usually much smaller than the time for significant changes in vapor density, we make the traditional quasi-steady-state assumption, so that

$$\nabla^2 \rho = 0. \tag{18}$$

For simple spherical particles of radius r, with the boundary conditions of $\rho = \rho_\infty$ at $r = \infty$ and $\rho = \rho_s$ at the particle surface ($r = a$), this Laplace equation has the following solution:

$$\rho(r) = \rho_\infty - \Delta\rho \frac{a}{r}, \tag{19}$$

where $\Delta\rho = \rho_\infty - \rho_s$ is the ambient excess vapor density.

The distribution of water vapor density ρ in the region surrounding a nonspherical ice crystal growing under quasi-steady-state conditions also satisfies the Laplace equation (18). However, the nonspherical shape of an ice crystal introduces complicated boundary conditions, which impose great difficulty in solving the Laplace equation. We therefore need to idealize the geometry of the ice crystals. Jayaweera and Cottis (1969) have shown that spheroids are good analogs for simple columnar and platelike ice crystals. As shown in Fig. 1, oblate spheroids resemble platelike ice crystals and prolate spheroids resemble columnar ice. In the discussion below, we will use spheroids to represent ice particles and apply the electrostatic analogy to describe the vapor density fields around the individual ice particles.

To solve the Laplace equation with spheroidal boundary conditions, it is convenient to use spheroidal coordinates instead of the spherical coordinates that were used in deriving (19). Since the spheroids are symmetric about the c axis, we can reduce the dimensions along the a and c axes to analogous dimensions in an elliptical coordinate system (μ, θ), as shown in Fig. 2. To change from elliptical coordinates to the Cartesian coordinates (x, y), corresponding to the a and c directions, respectively, we use the following conversion:

$$\mu = \frac{r_1 + r_2}{2}, \tag{20}$$

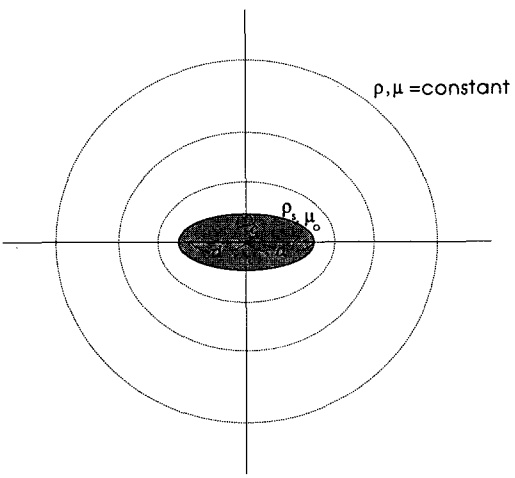

FIG. 2. Elliptical coordinate (μ, θ) and the constant μ surfaces. The shaded area represents the spheroidal approximation of an ice particle, while the constant μ contours represent constant vapor density isopleths around the ice crystals.

where

$$\left.\begin{aligned} r_1 &= \sqrt{(x+d)^2+y^2} \\ r_2 &= \sqrt{(x-d)^2+y^2} \\ d &= \sqrt{a^2-c^2} \end{aligned}\right\} \quad \text{(oblate spheroids)},$$

$$\left.\begin{aligned} r_1 &= \sqrt{x^2+(y+d)^2} \\ r_2 &= \sqrt{x^2+(y-d)^2} \\ d &= \sqrt{c^2-a^2} \end{aligned}\right\} \quad \text{(prolate spheroids)}.$$

Here, d is one-half the distance between the foci. Therefore, in elliptical coordinates, the constant ρ contours lie on constant μ surfaces as shown in Fig. 2. The solution of the Laplace equation, with boundary conditions of $\rho = \rho_\infty$ at $\mu = \infty$ and $\rho = \rho_s$ at $\mu = \mu_0$, can now be obtained in a form similar to (19):

$$\rho(\mu) = \rho_\infty - \Delta\rho \frac{\mu_0}{\mu}. \tag{21}$$

The vapor density gradient is thus

$$\frac{\partial\rho}{\partial\mu} = \Delta\rho \frac{\mu_0}{\mu^2}. \tag{22}$$

The vapor density gradients in Cartesian coordinates can then be expressed as

$$\frac{\partial\rho}{\partial x} = \frac{\partial\rho}{\partial\mu}\frac{\partial\mu}{\partial x}, \tag{23}$$

$$\frac{\partial\rho}{\partial y} = \frac{\partial\rho}{\partial\mu}\frac{\partial\mu}{\partial y}, \tag{24}$$

where, from (20),

$$\frac{\partial\mu}{\partial x} = \begin{cases} \dfrac{1}{2}\left(\dfrac{x+d}{\sqrt{(x+d)^2+y^2}} + \dfrac{x-d}{\sqrt{(x-d)^2+y^2}}\right) \\ \qquad \text{(oblate spheroids)} \\ \dfrac{1}{2}\left(\dfrac{x}{\sqrt{x^2+(y+d)^2}} + \dfrac{x}{\sqrt{x^2+(y-d)^2}}\right) \\ \qquad \text{(prolate spheroids)} \end{cases}$$

$$\frac{\partial\mu}{\partial y} = \begin{cases} \dfrac{1}{2}\left(\dfrac{y}{\sqrt{(x+d)^2+y^2}} + \dfrac{y}{\sqrt{(x-d)^2+y^2}}\right) \\ \qquad \text{(oblate spheroids)} \\ \dfrac{1}{2}\left(\dfrac{y+d}{\sqrt{x^2+(y+d)^2}} + \dfrac{y-d}{\sqrt{x^2+(y-d)^2}}\right) \\ \qquad \text{(prolate spheroids)} \end{cases}$$

To find the ratio of vapor density gradients over the basal faces ($x = 0$, $y = c$) to that over the prism faces ($x = a$, $y = 0$) in Eq. (14), one can combine (20), (21), (22), and (24) to get

$$\Phi \equiv \frac{\nabla\rho(0,c)}{\nabla\rho(a,0)} = \frac{\left(\dfrac{\partial\rho}{\partial y}\right)\Big|_{x=0,y=c}}{\left(\dfrac{\partial\rho}{\partial x}\right)\Big|_{x=a,y=0}} = \frac{\left(\dfrac{\partial\mu}{\partial y}\right)\Big|_{x=0,y=c}}{\left(\dfrac{\partial\mu}{\partial x}\right)\Big|_{x=a,y=0}}$$

$$= \begin{cases} \dfrac{\dfrac{1}{2}\left(\dfrac{c}{\sqrt{d^2+c^2}} + \dfrac{c}{\sqrt{d^2+c^2}}\right)}{\dfrac{1}{2}\left(\dfrac{a+d}{a+d} + \dfrac{a-d}{a-d}\right)} = \dfrac{c}{a} \\ \qquad \text{(oblate spheroids)} \\ \dfrac{\dfrac{1}{2}\left(\dfrac{c+d}{c+d} + \dfrac{c-d}{c-d}\right)}{\dfrac{1}{2}\left(\dfrac{a}{\sqrt{a^2+d^2}} + \dfrac{a}{\sqrt{a^2+d^2}}\right)} = \dfrac{c}{a} \\ \qquad \text{(prolate spheroids)}, \end{cases} \tag{25}$$

which is simply the *aspect ratio* $\phi \equiv c/a$.

Now, the ratio of the linear growth rates in (12) can be expressed simply as

$$\frac{dc}{da} = \Gamma(T)\phi \tag{26a}$$

or

$$\frac{d\ln c}{d\ln a} = \Gamma(T). \tag{26b}$$

By comparing this result (26a) with the derivative of the empirical relationship (3),

$$\frac{dc}{da} = \beta\eta a^{\beta-1} = \beta\frac{c}{a} = \beta\phi, \tag{27}$$

one may notice the resemblance between the theoretical result, (26a), and that from observations, (27). The differential forms of both formulas exhibit a direct proportionality between the ratio of the linear growth rates and the aspect ratio ϕ. Also, since β depends on the crystal type, which in turn depends on temperature, one can readily identify β as the temperature-dependent *inherent growth habit* Γ. In fact, the values of β from observational results correspond remarkably well with the experimental values of Γ, as shown in Fig. 3. The thick gray line and the dotted line in Fig. 3 indicate the inherent growth ratios, Γ, derived from the measure-

ments of Lamb and Scott (1972) and Sei and Gonda (1989), respectively. The shaded circles represent the values of β from various observational data. We can see a fairly good correlation, so it is suggested that the empirical parameter β is a direct reflection of the inherent growth habit $\Gamma(T)$ and is thus controlled by fundamental surface kinetic processes. The thin line in Fig. 3 represents a summary of the available information and is suggested as the inherent growth ratio to be used for the calculation of crystal shapes for temperatures between −30° and 0°C.

4. Ventilation effect

The empirical expression (3) fits the observational data quite well except for relatively large ice crystals. Figure 4 shows the general relationship between the lengths of the a and c axes of observed ice crystals (cf. Fig. 20 in Ono 1970), with the shaded area representing the spread of the data. A nearly perfect power law relationship is followed until the long axis reaches several hundred micrometers. Then, the growth seems to occur mostly along the long axes, reflecting the stage of limiting growth suggested by Miller and Young (1979).

Such a deviation from the power law behavior can be explained by the effect of ventilation on the diffusional growth. Recall that, from (14), the ratio of the vapor fluxes for a stationary ice crystal is proportional to the ratio of the vapor density gradients: $\Phi(c, a) = \nabla\rho_c/\nabla\rho_a$. However, as ice particles fall through the air, the effect of ventilation enhances the vapor fluxes, especially those toward the prominent edges of the ice crystals (Keller and Hallett 1982). If we let the effect of ventilation on the vapor flux ratio be f, Eq. (26a) can be modified as follows:

$$\frac{dc}{da} = \Gamma(T)\Phi(c, a) = \Gamma(T) f \phi, \qquad (28)$$

where f, in effect an asymmetry factor, is a function of a, c, and the properties of air. Although several studies exist on the overall effect of ventilation on crystal growth (e.g., Pitter 1974, 1980; Keller and Hallett 1982), the ratio f of the local ventilation factors for the a and c axes is not well known.

Nevertheless, we can derive a first-order approximation for f from existing knowledge. Based on the

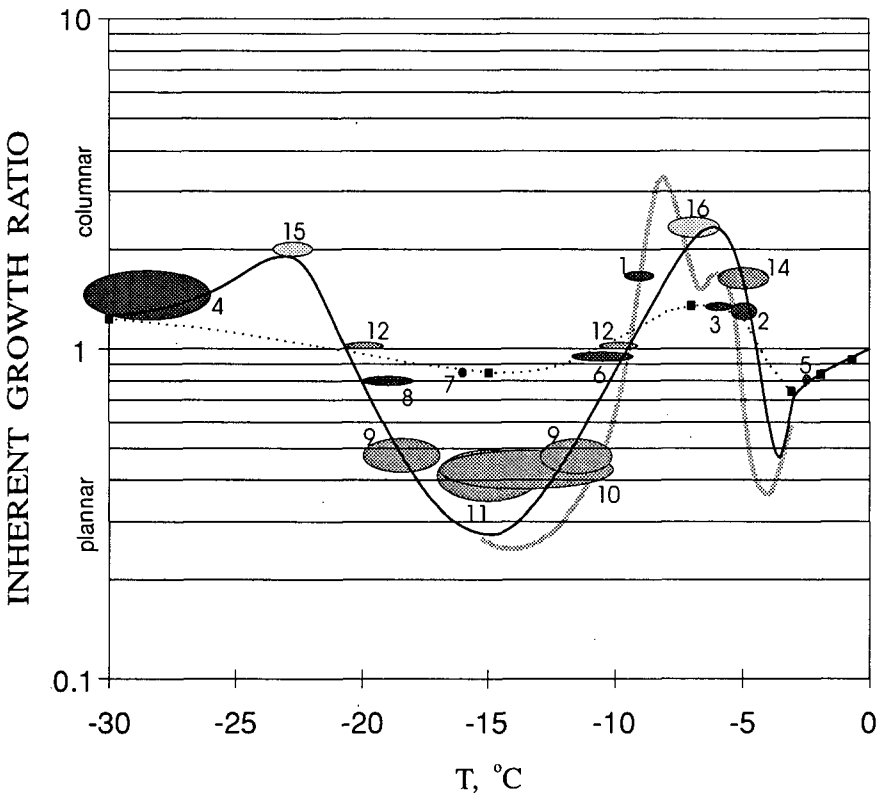

FIG. 3. Comparisons between the experimental and observational values of the inherent growth ratio. The thick line is from Lamb and Scott (1972); dotted line is from Sei and Gonda (1989) with actual data points denoted as filled squares. The shaded ellipses 1 to 8 are from Ono (1970), 9 to 14 from Auer and Veal (1970), 15 from Heymsfield and Knollenberg (1972), and 16 from Jayaweera and Ohtake (1974). The thin solid line is the best-fit values proposed in this study.

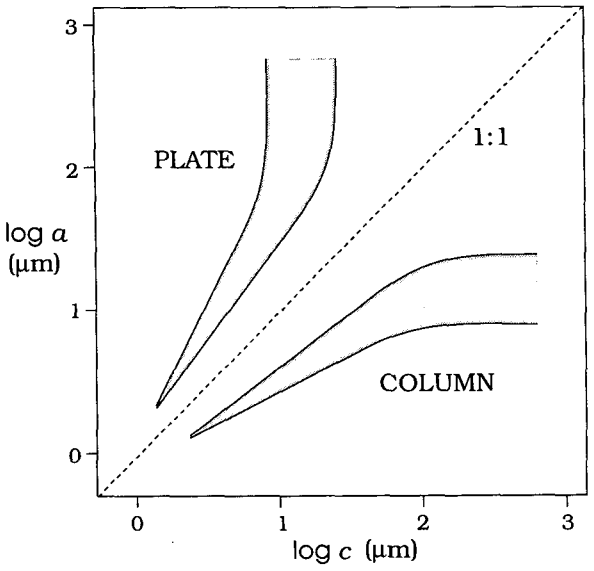

FIG. 4. Schematic diagram of the observed ice crystal axial ratio relationship.

results reported in the literature, Beard and Pruppacher (1971) expressed the overall (average) ventilation effect for the whole particle in the form of

$$\bar{f} = b_1 + b_2 X^{\gamma}, \tag{29}$$

where b_1, b_2, and γ are constants and $X = N_{Sc}^{1/3} N_{Re}^{1/2}$ is a function of the Schmidt number N_{Sc} and the Reynolds number N_{Re} of the particle. Hall and Pruppacher (1976) compiled data from Pitter et al. (1974) and other sources to give

$$b_1 = 1.0, \quad b_2 = 0.14, \quad \gamma = 2 \quad \text{for} \quad X \leq 1,$$

$$b_1 = 0.86, \quad b_2 = 0.28, \quad \gamma = 1 \quad \text{for} \quad X > 1. \tag{30}$$

For all practical purposes, we can use $\gamma = 1$ because the ventilation effect is important only when $X > 1$. The parameter X is proportional to the square root of the Reynolds number, which in turn is proportional to the characteristic length of the particle (Pitter et al. 1974). Thus, as a first approximation, we assume that the magnitude of the "local" ventilation effect is directly related to the relative dimensions of the crystal. That is, those parts of the crystal surface that extend farthest into the airstream experience the greatest benefits from ventilation. The local ventilation coefficient can then be related to the overall ventilation coefficient $\bar{f}$ by comparing the local radial dimension with r_0, the radius of a spherical particle having the same $\bar{f}$. The local ventilation coefficients for the c and a axes are therefore estimated as

$$f_c \approx b_1 + b_2 X^{\gamma} \left(\frac{c}{r_0}\right)^{1/2}, \tag{31}$$

$$f_a = b_1 + b_2 X^{\gamma} \left(\frac{a}{r_0}\right)^{1/2}. \tag{32}$$

The parameter f can thus be approximated as

$$f = \frac{f_c}{f_a} \approx \frac{b_1 + b_2 X^{\gamma} \left(\frac{c}{r_0}\right)^{1/2}}{b_1 + b_2 X^{\gamma} \left(\frac{a}{r_0}\right)^{1/2}}. \tag{33}$$

Figure 5 shows f as a function of the aspect ratio (c/a) and the spherical equivalent radius of the ice particles for the values of γ, b_1, and b_2 given by Hall and Pruppacher (1976). The value of f is near unity for particles that either are small or have an aspect ratio near unity. For large ice particles, f approaches the square root of the aspect ratio.

Now, for completeness, let us combine f with Γ in (28) so that the relationship between a and c can reflect the ventilation effect and still be expressed in a power law relationship similar to that given in (3):

$$c = \eta a^{\Gamma^*}. \tag{34}$$

Here, $\Gamma^* = \Gamma(T) f$ may be thought of as the ventilation-influenced growth habit. From this formula, we are able to reconstruct the observed relationship between the a and c axis lengths, as shown in Fig. 6. For these computations, the particles were initially taken to be spherical with a radius of 1 μm. The subsequent growth of the particles was assumed to abide by the specified inherent growth habit Γ, as modified by the ventilation effect through (34). The relationship between the a and c axes is initially loglinear, but it gradually deviates from this dependence as the sizes become large and the local ventilation effects become important. Figure 6 shows great similarity to the observational results in Fig. 20 of Ono (1970) and Fig. 4. Note that the spread of the observational data could be due in part to the variations of air temperature and, therefore, to continually varying values of $\Gamma(T)$.

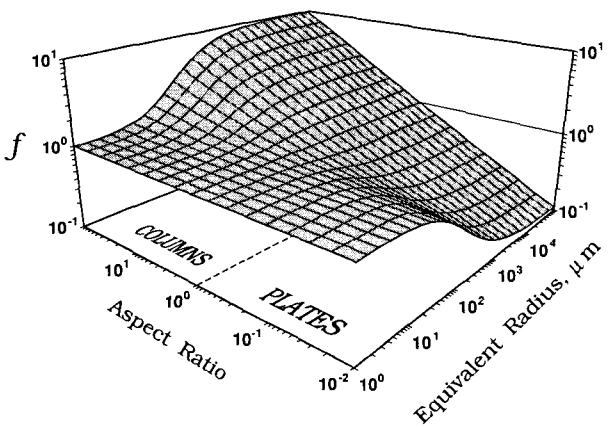

FIG. 5. The ratio of local ventilation coefficients for the c axis to that at the a axis as a function of the aspect ratio and equivalent radius of the ice particles.

5. Change of aspect ratio and mass growth

Equation (26) describes the relative distribution of water fluxes to the main crystallographic faces from a theoretical approach. Together with the conventional mass growth equation introduced in this section, we are able to derive a relatively complete description of the depositional growth of ice. However, it is first convenient to convert the linear growth rates into the *change of aspect ratio* by taking the logarithmic differential of the volume of a spheroid, $V = \frac{4}{3}\pi a^3\phi$:

$$d\ln V = 3d\ln a + d\ln\phi. \tag{35}$$

The differential of ϕ $(=c/a)$ can be expanded into

$$d\phi = \frac{1}{a}dc - \frac{c}{a^2}da = \left(\frac{dc}{da} - \phi\right)d\ln a. \tag{36}$$

Now, by replacing dc/da here with (26a) and combining the last two equations, we derive the expression for the change of aspect ratio as a function of the volume change:

$$d\ln\phi = \frac{\Gamma - 1}{\Gamma + 2}d\ln V. \tag{37}$$

The temperature-dependent parameter Γ determines the direction of change of ϕ. For example, in the columnar temperature regime where $\Gamma > 1$, the shape of an ice crystal will become more (less) columnar during growth (decay) regardless of its original shape. This means that whereas the primary habit is controlled by temperature, the magnitude of the change of ϕ is determined by both Γ and the volume change. To consider the ventilation effect, one need only replace Γ with $\Gamma^* = f\Gamma$. The change of volume can be derived from the mass growth rate and the deposition density, an operation that is discussed next.

The diffusional mass growth of an ice particle follows in concept very closely that for drop growth. If we apply the electrostatic analogy in spheroidal coordinates, the mass flux over the surface A of the ice particle, based on Gauss' law and Fick's law of diffusion, is given by

$$\frac{dm}{dt} = \int_A \bar{f}D_v\nabla\rho\cdot\mathbf{n}dA = 4\pi C\bar{f}D_v\Delta\rho, \tag{38}$$

where C is the electrostatic capacitance, and $\mathbf{n}$ is the unit vector pointing perpendicular to the surface. For oblate spheroids ($\phi < 1$), the capacitance is given by

$$C = \frac{a\epsilon}{\sin^{-1}\epsilon} = \frac{d}{\sin^{-1}\epsilon}, \tag{39}$$

where the eccentricity $\epsilon = \sqrt{1 - c^2/a^2} = \sqrt{1 - \phi^2}$ and the semilength of the foci $d = \sqrt{a^2 - c^2} = a\epsilon$. For prolate spheroids ($\phi > 1$),

$$C = \frac{c\epsilon}{\ln[(1+\epsilon)\phi]} = \frac{d}{\ln[(1+\epsilon)\phi]}, \tag{40}$$

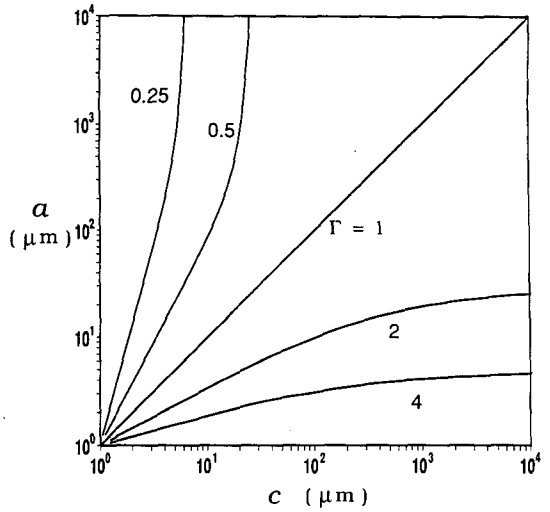

FIG. 6. The calculated lengths of c and a axes of ice particles grown at various values of the inherent growth habit Γ.

where $\epsilon = \sqrt{1 - a^2/c^2} = \sqrt{1 - \phi^{-2}}$ and $d = \sqrt{c^2 - a^2} = c\epsilon$. When $d = 0$, the particle is spherical and C reduces to the radius r of the particle. Detailed derivations of (39) and (40) can be found in Snow (1954, p. 9, pp. 55–57). Measurements by McDonald (1963) of the capacitances of metal models of snow crystals agree very well with the above theoretical values for the idealized geometries.

The change of particle volume is in general related simply to the mass change. Thus,

$$dV = \frac{1}{\rho_{dep}}dm, \tag{41}$$

where ρ_{dep} is the mass density at the time of deposition.

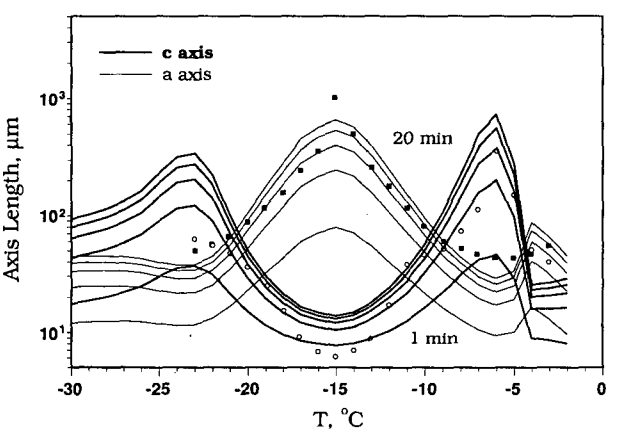

FIG. 7. Evolution of the a (thin lines) and c (thick lines) axes lengths of single crystals after 1, 5, 10, 15, and 20 min growth. These are compared with those observed by Takahashi et al. (1991) for 10 min growth, shown by the filled squares (a axis) and open circles (c axis).

Miller and Young (1979) have expressed the deposition density as functions of temperature and supersaturation using the experimental data of Fukuta (1969). An alternative formula that is based on the same experimental results but expressed in a less complicated form is provided here for the deposition density (g cm^{-3}):

$$\rho_{dep} = 0.91 \exp[-3 \cdot \max(\Delta\rho - 0.05, 0)/\Gamma(T)], \quad (42)$$

where $\Delta\rho$ is the excess vapor density (in g m^{-3}). The change of the apparent volume due to depositional growth can thus be calculated from the mass growth equation (38) and the deposition density through (41). In turn, the change in the aspect ratio can be calculated from (37). The changes in the lengths of the c and a axes may then be calculated explicitly in terms of the volume change from combinations of (35) through (37):

$$d \ln c = \left(\frac{\Gamma}{\Gamma + 2}\right) d \ln V, \quad (43)$$

$$d \ln a = \left(\frac{1}{\Gamma + 2}\right) d \ln V. \quad (44)$$

In effect, this scheme offers a self-consistent and physically based way for determining how any given increment in water mass should be distributed among the basal and prism faces during the depositional growth of ice crystals. Moreover, the approach allows the growth and habits of ice crystals to adapt to the locally changing conditions of temperature and supersaturation in a way that reflects their prior growth histories.

6. Simulation of the growth and shape changes of ice crystals

a. *Growth under fixed conditions*

The parameterization scheme described above was used to simulate the depositional growth of single ice crystals for fixed ambient conditions. Individual calculations for the growth of ice crystals, initially spherical and 1 μm in radius, were made for each 1°C from −30° to −1°C, all at liquid water saturation and an air pressure of 1000 mb. The transfer of water mass and heat between the ice crystals and air during growth was calculated using the treatment of Chen (1992, p. 177). The ventilation effect is considered by assuming that the crystals fall at their terminal velocities, as calculated according to the formulas of Böhm (1989, 1992).

Figure 7 shows the calculated lengths along the a (thin lines) and c (thick lines) axes of the ice crystals after 1, 5, 10, 15, and 20 min of growth. Primary growth maxima occur along the a and c axes near −15°C and −6°C, temperatures that correspond to the dendrite and needle regimes, respectively. Secondary growth maxima are also found near −4° and −23°C along the a and c axes, respectively. While the growths along the major axes are at their maximum, the growths along the minor axes are at their minimum. The general features of the predictions are in reasonable agreement with the measurements of Takahashi et al. (1991), shown in Fig. 7 by the filled squares (a axis) and open circles (c axis) for 10 min of growth. The differences between the predicted and the measured values are well within the discrepancies found among various experimental results (cf. Fukuta 1969; Ryan et al. 1976; Kowa 1981; Gong and Fukuta 1985; Takahashi and Fukuta 1988). Differences between the simulated and measured results could arise from acknowledged uncertainties in Γ used in the model, as well as from uncertainties in the laboratory studies. We must also bear in mind the limitations imposed by the relatively crude approximation to crystal shapes as spheroids needed by the theory.

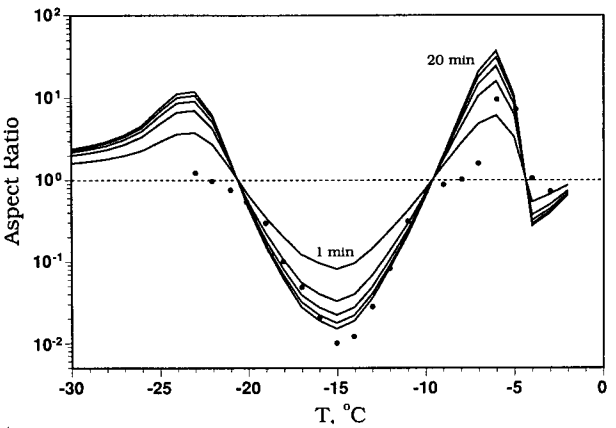

FIG. 8. Same as Fig. 7 except for the crystal aspect ratios. The closed circles are laboratory results from Takahashi et al. (1991) for 10 min growth.

The aspect ratios of the crystals, as shown in Fig. 8, became more extreme with the growth. The alternating plate–column–plate–column temperature dependence of crystal habits is evident for the temperature range of −30° to 0°C. Note that the shape asymmetry, as measured by $|\log\phi|$, of ice crystals in the warm column regime (−6°C) becomes comparable to that in the cold plate regime (−15°C), even though the columns grew slower in mass and have smaller "inherent asymmetry" (e.g., $|\log\Gamma|$). This behavior arises because the *fractal dimension*, ζ, of columnar crystals is inherently smaller than that of planar crystals, as will be shown later in (49) and (50), so that the masses of columns are more weakly dependent on their sizes. The simulations are compared with the measurements of Takahashi et al. (1991) for 10 min of growth, as shown by the filled circles in Fig. 8. Again, the general features are very similar, with minor discrepancies in their magnitudes.

The predicted masses of crystals grown under fixed conditions are shown in Fig. 9. The primary and secondary growth maxima occur near −15° and −6°C, respectively, where the crystals are most asymmetrical. The mass growth of ice crystals is linearly dependent on the vapor density excess, so one might expect maximum growth to coincide with the maximum excess vapor density. Yet, the actual maximum growth does not occur at this higher temperature because of the nonlinear dependence of the crystal growth on the inherent growth ratio Γ. Moreover, the nonlinearity is greater for columnar crystals than for planar ice due to their different fractal dimensions, ζ. Thus, other factors remaining constant, planar crystals ($2 < \zeta < 3$) grow faster in mass than spherical crystals ($\zeta = 3$), but slower than columnar crystals ($1 < \zeta < 3$) that have the same "inherent asymmetry," $|\log\Gamma|$. Another factor that may contribute to faster growth is a low deposition density, shown by Fukuta (1969) to have minima at −6° and −16°C. Again, the predicted mass growths are in fairly good agreement with the laboratory measurements of Takahashi et al. (1991), as indicated by the closed circles in Fig. 9 for 10 min of growth. Good agreements were also found upon comparing our results for fixed conditions to the simulations of Hindman and Johnson (1972), Miller and Young (1979), and Redder and Fukuta (1989).

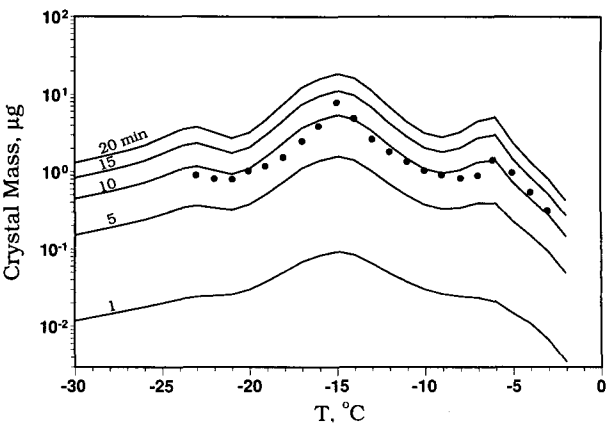

FIG. 9. Same as Fig. 7 except for the crystal masses. The closed circles are laboratory results from Takahashi et al. (1991) for 10 min growth.

b. Adaptive growth

An adaptive parameterization of ice crystal habits, such as that developed in this paper, finds its greatest utility in models that permit the crystal shapes to change with time in a predictive way. Here, we demonstrate this parameterization scheme by using it in a detailed microphysical model that simulates the formation of ice crystals in a rising air parcel. This microphysical model applies a particle framework that simultaneously and independently categorizes ice particles according to their masses and to their shapes. A method-of-moments type scheme was used to calculate the transfer of particles between categories. Detailed descriptions of this multicomponent particle framework have been provided by Chen and Lamb (1992a,b: 1994), as well as by Chen (1992). For this simulation, the liquid-phase microphysics has been treated in full detail. However, riming and aggregation processes have been excluded from the ice-phase microphysics so that only the pure effect of diffusional growth is shown. Several ice nucleation processes are included in the model, but only heterogeneous deposition nucleation is important in the present case. The supersaturation-dependent formula of Huffman (1973) was used to calculate the number concentration of ice crystals nucleated through heterogeneous deposition. All ice particles formed had an initial aspect ratio of unity and an equivalent spherical radius of 1 μm.

The air parcel was assumed to ascend adiabatically at a speed of 1 m s^{-1}, forming a cloud base near 0°C and 800 mb. Figures 10a and 11a show the simulated ice crystal distribution at different times in the particle framework, with water mass and aspect ratio (shape) used as the two coordinates. These graphs are transformed into Figs. 10b and 11b with the *a* and *c* axis lengths as the coordinates, so that one can compare them with Figs. 4 and 6. Figure 10 shows the distribution of ice crystals at 18 min simulation time, when the air temperature was about −5°C. Up to this time, the ice particles formed and grew in the planar ice regime. The smaller, newly formed ice crystals grew with aspect ratios close to unity. As the planar ice crystals grew larger, they became flatter and exhibited smaller aspect ratios. Some spreading of the distribution is apparent because of the temporal variation of temperature and, therefore, of the inherent growth habits. Figure 11 shows the distributions of the ice crystal population at 22 min simulation time, when the air temperature was about −7°C. One can see that no new planar ice crystals were being formed, and that all planar ice crystals had equivalent radii greater than 10 μm. The particles that nucleated at temperatures below about −5°C (after 18 min) were formed in the columnar ice regime, as shown on the right (lower right) of Figure 11a (11b). The distribution of the columnar ice is similar to that of the planar ice crystals in Fig. 10 except for the opposite slope.

The distribution of the planar ice formed earlier, however, deviates from the expected power law relationship. The aspect ratio of these planar crystals did not become smaller (more planar) as they grew larger. Such a phenomenon results from the change of the inherent growth habits, from a planar growth regime to a columnar growth regime, during this period of time. The change of the inherent growth habits tended to force the whole distribution to shift toward the columnar regime. Although most of the larger and flatter ice crystals were able to maintain their planar shapes, some

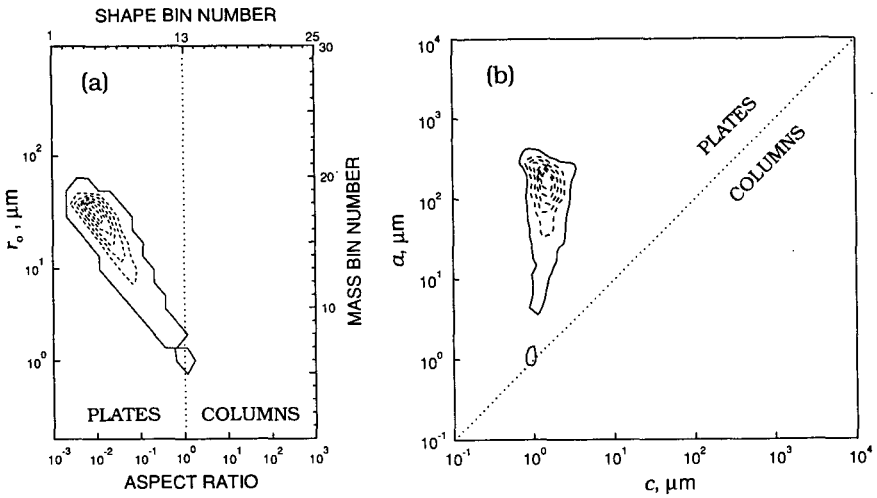

FIG. 10. Simulated ice crystal distribution at 18 min simulation time, with air temperature at about −5°C. (a) Ice crystal distribution function in m (water mass) and ϕ (shape) coordinates; the right axis is the water mass category number, with corresponding equivalent radius shown on the left; the top axis is the shape category number, with the corresponding aspect ratio shown on the bottom. The contour interval is 0.002 mol^{-1} per unit log$m$ and logϕ. (b) Ice crystal distribution function in a and c axial length coordinates. The contour interval is 0.2 mol^{-1} per unit log$a$ and log$c$.

of the smaller crystals changed their habits and became columnar. These smaller crystals that changed habits had never experienced values of $\Gamma(T)$ that were much smaller than unity. Note, however, that under the relatively high supersaturation conditions found in some atmospheric clouds, a shift from columnar growth to planar growth would not result in fatter columns; rather, "capped columns" would be more likely to form (Magono and Lee 1966). Similarly, a shift from planar growth to columnar growth might result in "crown crystals" [needles attached to the edges of plates; Nakaya (1954)]. Such complicated secondary crystal habits are described only implicitly by our parameterization, as it is based on spheroids. Nevertheless, the aspect ratio of real ice crystals can be defined as the ratio of the "maximum" crystal dimensions, while the void space within a circumscribed spheroid is accounted for by the low deposition density. The polycrystalline structure of side planes or bullet rosettes that form from frozen drops at low temperatures (Ma-

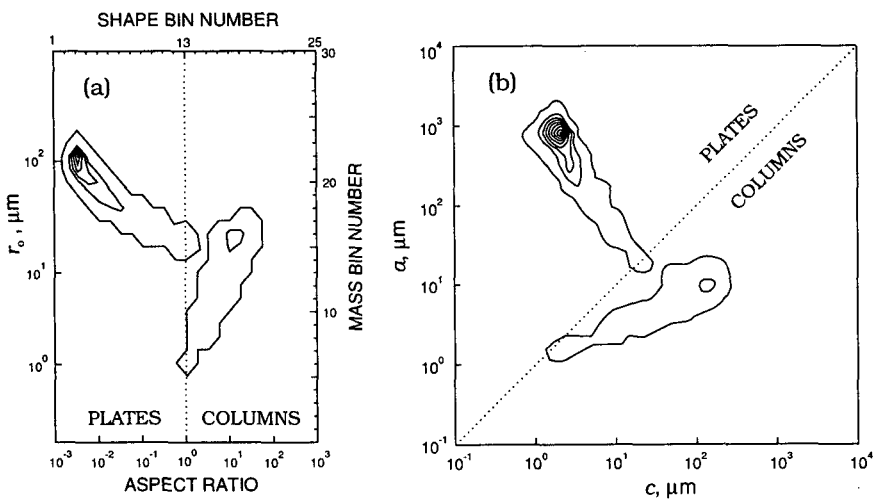

FIG. 11. Same as Fig. 10 except at 22 min simulation time. The air temperature is −7°C. The contour intervals are 0.02 mol^{-1} per unit log$m$ and logϕ (a) and 2 mol^{-1} per unit log$a$ and log$c$ (b).

gono and Lee 1966; Lee 1972; Furukawa 1982) may be approximated in a similar way. However, a redefinition of the "inherent growth habit" and a proper description for the deposition density might be needed for such spatial forms.

7. Mass–dimension relationships

The two-component particle framework shown in the previous section provides a way to simulate the size and shape spectra of ice crystals in detail. However, it is possible to use some simplified parameterization schemes in conventional microphysical models to account for the effect of shape on the ice-phase microphysics. Mitchell (1988) applied the expression for the mass–dimension relationships of Locatelli and Hobbs (1974) to represent the mass of ice particles:

$$m = \xi D^{\zeta}, \tag{45}$$

where D is the maximum dimension of the ice particles and ξ and ζ are constants that depend on the type and shape of the ice particles. Davis (1974), as well as Mitchell et al. (1990), derived values for ξ and ζ for pristine single crystals from observational data. As with the shape parameterization (3), however, no interpretation was provided to account for the mass–dimension relationship and its coefficients. Here, we extend our theoretical analysis to derive the mass–dimension relationship (45) for pristine single crystals and show that the exponent ζ, the fractal dimension, is also controlled by the inherent growth ratio Γ.

By applying the relationship between the a and c axes given in (34), we can express the mass of an ice crystal approximated by a spheroid,

$$m = \frac{4}{3}\pi\rho_i a^2 c, \tag{46}$$

in terms of the semilength of its long axis (half of the maximum dimension):

$$m = \left(\frac{4}{3}\pi\rho_i\eta^{-2/\Gamma^*}\right)c^{2/\Gamma^*+1},$$

for columnar ice $(D = 2c)$ (47)

$$m = \left(\frac{4}{3}\pi\rho_i\eta\right)a^{2+\Gamma^*},$$

for planar ice $(D = 2a)$ (48)

where ρ_i is the apparent density of the ice particle. The above mass–dimension relationships are in a form very similar to (45) with the following equivalences:

$$\xi = \frac{2}{3}\pi\rho_i(2\eta)^{-2/\Gamma^*}, \quad \zeta = \frac{2}{\Gamma^*} + 1,$$

for columnar ice $(\Gamma > 1)$ (49)

$$\xi = \frac{2^{-\Gamma^*}}{3}\pi\rho_i\eta, \quad \zeta = 2 + \Gamma^*,$$

for planar ice $(\Gamma < 1)$. (50)

We can now see that the exponent in (45) is an explicit function of the inherent growth ratio Γ. Since $\Gamma > 1$ for columnar ice and $\Gamma < 1$ for planar ice, the value of ζ is always less than 3 for nonspherical ice particles. The more the crystal deviates from a sphere, the smaller the values of ζ will be until the limiting values of 1 (columns) or 2 (plates) are reached. Thus, the fractal dimension, ζ, of pristine single crystals is controlled by the inherent growth habits, Γ. Note that ζ is always greater than 2 for planar ice, but it can be less than 2 for columnar ice. Again, as noted earlier, the fractal dimension of columnar crystals is always smaller than that of planar crystals having a similar "inherent asymmetry," $|\log\Gamma|$. Figure 12 shows the comparison between the values of Γ estimated from the observed values of ζ for small crystals using (49) and (50) (shaded rectangles), and the values of Γ shown in Fig. 3 (curve). One can see that a fairly good agreement exists. The observed values of ζ for large crystals ($D \gtrsim 300$ μm) are somewhat different from those for small crystals (not shown), possibly due to the ventilation effect.

If not used in their differential forms, (34) and (45) require knowledge of the coefficients η and ξ, respectively. Although our analysis does not provide a value for η, one can gain an estimate from the fact that very small ice crystals are nearly isometric (Miller and

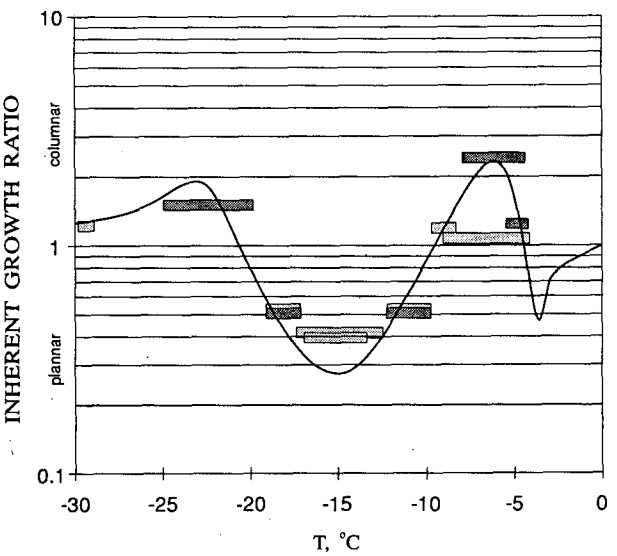

FIG. 12. Comparisons between the inherent growth ratios Γ derived through the mass–dimension relationship and that in Fig. 3. Light-shaded areas are values estimated from the data by Davis (1974), and dark-shaded areas are estimated from the data in Mitchell et al. (1990). The solid line is the best-fit Γ in Fig. 3.

Young 1979). For a small, nearly spherical ice crystal with radius r_Δ, we can let $a = c = r_\Delta$ in (34) to get

$$\eta \approx r_\Delta^{(1-\Gamma)}. \quad (51)$$

By inserting the values of η for planar ice crystals from Auer and Veal (1970) and Davis (1974) into (51), one finds that r_Δ lies consistently between 0.7 and 2.6 μm and well within the isometric growth regime. However, using the data from Auer and Veal (1970), Heymsfield and Knollenberg (1972), Jayaweera and Ohtake (1974), and Davis (1974), one finds that r_Δ for columnar ice crystals ranges from very small values to about 30 μm. Such a large spread is not surprising because the intercept, $\log\eta$, of the log-linear function (34) is very susceptible to error when extrapolated to very small sizes.

8. Summary and conclusions

Through a theoretical approach, the shape of an ice crystal due to depositional growth has been demonstrated to be controlled by two factors. The first factor, which is a surface kinetic effect, is the difference in the condensation coefficients of the prism and basal faces of the ice crystal. The inherent growth ratio, defined as the ratio of the basal-face and prism-face condensation coefficients, is primarily a function of temperature and can be obtained from laboratory results. The second factor, which is a gas-phase mass transport effect, is the difference in the fluxes of vapor to the prism and basal faces of the ice crystals. The vapor density gradients around a nonspherical ice crystal are distorted both by the shape of the particle and by the nonuniform distribution of condensation coefficients across the crystal surface. Also, ventilation effects enhance the vapor density gradients near the prominent edges of the ice crystals as they grow larger than about 100 μm along the major dimension.

From the theoretical analysis, the shape of an ice crystal grown by vapor deposition can be parameterized into a power law form that shows great resemblance to some of the empirical formulas that have been obtained from observational data. Therefore, a physical explanation for the observed power law relationship is provided by the theoretical analysis. The exponent of the power law relationship turns out to be identical to the inherent growth ratio. The observed axial relationship, however, deviates from a power law at large crystal sizes, an effect that can be explained by preferential ventilation and a further enhancement of the vapor flux to the prominent faces. By applying the power law relationship for crystal shapes, one can also develop a set of mass–dimension relationships that shows great resemblance to those obtained from observational data. The coefficients of the mass–dimension relationship also are found to be controlled by the inherent growth ratio. The analysis done in this study may thus lead to an alternative method for measuring the inherent growth ratio indirectly through observed dimensional relationships.

The parameterization scheme developed here has been used to simulate the growth of single crystals under both fixed and time-varying ambient conditions. The known variations of crystal habit with temperature were clearly reproduced, and the predictions of crystal axial lengths and masses are in reasonable agreement with laboratory measurements taken at various fixed temperatures. The scheme was also applied in a detailed microphysical model to simulate the time evolution of the size and shape distribution of ice particles in an idealized cloud. The shapes of the ice crystals are shown to respond appropriately to the systematic change of air temperature and, therefore, adapt to the change in the inherent growth ratio. As the air temperature decreased, causing a switch to a different habit regime, crystals that already had aspect ratios much different from unity tended to retain their original habits whereas younger crystals tended to change their primary habits. Even though the ratios of the axial lengths of ice particles tend to follow a power law relationship, the variation of air temperature (and, thus, the inherent growth ratio) may cause the size and shape distribution to broaden and deviate from the power-law relationship.

The parameterization scheme developed here on theoretical grounds provides a self-consistent way for understanding the evolution of ice crystal sizes and shapes, as well as their roles in cloud processes. The detailed size and shape information obtained from the microphysical simulation may lead to improvements over traditional parameterizations of bulk water microphysical processes in precipitating clouds and radiative interactions in cirrus clouds.

Acknowledgments. This work was supported in various parts by the Department of Energy under Grant DE-FG02-90ER61071 and the National Science Foundation under Grant ATM-8919837. One author (J. P. Chen) wishes to acknowledge support from the Earth System Science Center, College of Earth and Mineral Sciences, for a fellowship and for the use of its CRAY-YMP computer. The detailed comments and suggestions of an anonymous reviewer are appreciated, as are discussions with Jon Nelson and Marcia Baker.

REFERENCES

Auer, A. H., Jr., and D. L. Veal, 1970: The dimension of ice crystals in natural clouds. *J. Atmos. Sci.*, **27**, 919–926.

aufm Kampe, H. J., H. K. Weickmann, and J. J. Kelly, 1951: The influence of temperature on the shape of ice crystals growing at water saturation. *J. Meteor.*, **8**, 168–174.

Beard, K. V., and H. R. Pruppacher, 1971: A wind tunnel investigation of the rate of evaporation of small water drops falling at terminal velocity in air. *J. Atmos. Sci.*, **28**, 1455–1464.

Böhm, H. P., 1989: A general equation for the terminal fall speed of solid hydrometeors. *J. Atmos. Sci.*, **46**, 2419–2427.

——, 1992: A general hydrodynamic theory for mixed-phase microphysics. Part I: Drag and fall speed of hydrometeors. *Atmos. Res.*, **27**, 253–274.

Burton, W. K., N. Cabrera, and F. C. Frank, 1951: The growth of crystals and the equilibrium structure of their surfaces. *Phil. Trans. Roy. Soc. London,* **A243,** 299–358.

Chen, J.-P., 1992: numerical simulations of the redistribution of atmospheric trace chemicals through cloud processes. Ph.D. dissertation, The Pennsylvania State University, University Park, PA, 342 pp.

——, and D. Lamb, 1992a: The effect of cloud microphysics on the composition of rain. *Precipitation Scavenging and Atmosphere-Surface Exchange,* S. E. Schwartz and W. G. N. Slinn, Eds., Hemisphere Publishing, 51–62.

——, and ——, 1992b: The evolution of saturation ratio. Preprints, *11th Int. Conf. on Clouds and Precipitation,* Montreal, Canada, ICCP/IAMAP, 322–325.

——, and ——, 1993: Simulation of cloud microphysical and chemical processes using a multicomponent framework, Part I. Description of the microphysical model. *J. Atmos. Sci.,* in press.

Cotton, W. R., 1972: Numerical simulation of precipitation development in supercooled cumuli—Part II. *Mon. Wea. Rev.,* **100,** 764–784.

Davis, C., 1974: The ice-nucleating characteristics of various AgI aerosols. Ph.D. thesis, University of Wyoming, Laramie, Wyoming, 267 pp.

Fuchs, N. A., 1959: *Evaporation and Droplet Growth in Gaseous Media.* Pergamon, 72 pp.

Fukuta, N., 1969: Experimental studies on the growth of small ice crystals. *J. Atmos. Sci.,* **26,** 522–531.

——, 1980: Development of fast falling ice crystals in clouds at −10°C and its consequences in ice phase processes. *Proc. 8th Int. Conf. on Cloud Physics,* Clermont-Ferrand, France, ICCP/IAMAP, 97–100.

——, L. R. Neubauer, and D. D. Erickson, 1979: Laboratory studies of organic ice nuclei smoke under simulated seeding conditions. Final Report to National Science Foundation under Grant ENV77-15346.

Furukawa, Y., 1982: Structures and formation mechanisms of snow polycrystals. *J. Meteor. Soc. Japan,* **60,** 535–547.

Gong, N., and N. Fukuta, 1985: Supercooled cloud tunnel studies of ice crystal growth for extended periods of time. *Plateau Meteor.,* **4,** 293–302.

Hall, W. D., and H. R. Pruppacher, 1976: The survival of ice particles falling from cirrus clouds in subsaturated air. *J. Atmos. Sci.,* **33,** 1995–2006.

Hallett, J., and B. J. Mason, 1958: The influence of temperature and supersaturation on the habit of ice crystals grown from the vapor. *Proc. Roy. Soc. London,* **A247,** 440–453.

Heymsfield, A. J., and R. G. Knollenberg, 1972: Properties of cirrus-generating cells. *J. Atmos. Sci.,* **29,** 1358–1366.

Hidy, G. M., and J. R. Brock, 1970: The dynamics of aerocolloidal systems. *International Reviews in Aerosol Physics and Chemistry, Vol. 1,* Pergamon, 379 pp.

Hindman, E. E., II, and D. B. Johnson, 1972: Numerical simulation of ice particle growth in a cloud of supercooled water droplets. *J. Atmos. Sci.,* **29,** 1313–1321.

Houghton, H. G., 1950: A preliminary quantitative analysis of precipitation mechanisms. *J. Meteor.,* **7,** 363–369.

Huffmann, P. J., 1973: Supersaturation spectra of AgI and natural ice nuclei. *J. Appl. Meteor.,* **12,** 1080–1082.

Jayaweera, K. O. L. F., and R. E. Cottis, 1969: Fall velocities of plate-like and columnar ice crystals. *Quart. J. Roy. Meteor. Soc.,* **95,** 703–709.

——, and T. Ohtake, 1974: Properties of columnar ice crystals precipitating from layer clouds. *J. Atmos. Sci.,* **31,** 280–286.

Jeffreys, H., 1918: Some problems of evaporation. *Philos. Mag.,* **35,** 270–280.

Keller, V. W., and J. Hallett, 1982: Influence of air velocity on the habit of ice crystal growth from the vapor. *J. Crystal Growth,* **60,** 91–106.

Kobayashi, T., 1961: The growth of snow crystals at low supersaturations. *Philos. Mag.,* **6,** 1363–1370.

Kowa, M. W., 1981: Determination of ice crystal growth parameters in a supercooled cloud tunnel. M.S. thesis, University of Utah, 127 pp.

Kuroda, T., 1982: Growth kinetics of ice single crystal from vapour phase and variation of its growth form. *J. Meteor. Soc. Japan,* **60,** 520–533.

——, and R. Lacmann, 1982: Growth kinetics of ice from the vapour phase and its growth forms. *J. Crystal Growth,* **56,** 189–205.

Lamb, D., and P. V. Hobbs, 1971: Growth rates and habits of ice crystals grown from the vapor phase. *J. Atmos. Sci.,* **28,** 1506–1509.

——, and W. D. Scott, 1972: Linear growth rates of ice crystals grown from the vapor phase. *J. Crystal Growth,* **12,** 21–31.

——, and ——, 1974: The mechanism of ice crystal growth and habit formation. *J. Atmos. Sci.,* **31,** 570–580.

Lee, C. W., 1972: On the crystallographic orientation of spatial branches in natural polycrystalline snow crystals. *J. Meteor. Soc. Japan,* **50,** 171–180.

Locatelli, J. D., and P. V. Hobbs, 1974: Fall speeds and masses of solid precipitation particles. *J. Geophys. Res.,* **79,** 2185–2197.

Magono, C., and C. W. Lee, 1966: Meteorological classification of natural snow crystals. *J. Fac. Sci.,* Hokkaido Imp. Univ., [VII], **2,** 321–335.

Mason, B. J., 1953: The growth of ice crystals in a supercooled water cloud. *Quart. J. Roy. Meteor. Soc.,* **79,** 104–111.

——, 1993: Growth habits and growth rates of snow crystals. *Proc. Roy. Soc. London,* **A441,** 3–16.

Maxwell, J. C., 1878: Diffusion. *Encyclopedia Britannica,* 9th ed., 214–221.

McDonald, J. E., 1963: Use of the electrostatic analogy in studies of ice crystal growth. *Z. Angew. Math. Phys.,* **14,** 610–619.

Miller, T. L., and K. C. Young, 1979: A numerical simulation of ice crystal growth from the vapor phase. *J. Atmos. Sci.,* **36,** 458–469.

Mitchell, D. L., 1988: Evolution of snow-size spectra in cyclonic storms. Part I: Snow growth by vapor deposition and aggregation. *J. Atmos. Sci.,* **45,** 3431–3451.

——, R. Zhang, and R. L. Pitter, 1990: Mass–dimensional relationships for ice particles and the influence of riming on snowfall rates. *J. Appl. Meteor.,* **29,** 153–163.

Nakaya, U., 1954: *Snow Crystals: Natural and Artificial.* Harvard University Press, 510 pp.

——, and Y. Sakido, 1936: General classification of snow crystals and their frequency of occurrence. *J. Fac. Sci.,* Hokkaido Imp. Univ., [II], **1,** 243–264.

Nordenskiöld, G., 1893: The inner structure of snow crystals. *Nature,* **48,** 592–594.

Ono, A., 1969: The shape and riming properties of ice crystals in natural clouds. *J. Atmos. Sci.,* **26,** 138–147.

——, 1970: Growth mode of ice crystals in natural clouds. *J. Atmos. Sci.,* **27,** 649–658.

Pitter, R. L., 1980: Convective diffusion and ice crystal habit. *J. Rech. Atmos.,* **14,** 281–288.

——, H. R. Pruppacher, and A. E. Hamielec, 1974: A numerical study of the effect of forced convection on mass transport from a thin oblate spheroid of ice in air. *J. Atmos. Sci.,* **31,** 1058–1066.

Pruppacher, H. R., and J. D. Klett, 1978: *Microphysics of Clouds and Precipitation.* D. Reidel, 714 pp.

Redder, C. R., and N. Fukuta, 1989: Empirical equations of ice crystal growth microphysics for modeling and analysis, I. Mass and dimensions. *Atmos. Res.,* **24,** 247–272.

Rooth, C., 1957: On a special aspect of the condensation process and its importance in the treatment of cloud particle growth. *Tellus,* **9,** 372–377.

Ryan, B. F., E. F. Wishart, and D. E. Shaw, 1976: The growth rate and densities of ice crystals between −3°C and −21°C. *J. Atmos. Sci.,* **33,** 842–850.

Sei, T., and T. Gonda, 1989: The growth mechanism and the habit change of ice crystals growing from the vapor phase. *J. Crystal Growth,* **94,** 697–707.

Shaw, D., and B. J. Mason, 1955: The growth of ice crystals from the vapour. *Philos. Mag.,* **46,** 249–262.

Snow, C., 1954: Formulas for computing capacitance and inductance. Natl. Bur. Stand. Circ. 544. Washington, DC, U.S. Dept. Commerce, 69 pp.

Stefan, M. J., 1873: Über die Verdampfung aus einem kreisfömig oder elliptisch begrenzten Becken. Wien Akad. Sci. Sitzungs Ber., *Math. Naturw.,* **Kl. 68, 2 Abt.,** 943–954.

Stephens, G. L., S.-C. Tsay, P. W. Stackhouse, Jr., and P. J. Flatau, 1990: The relevance of the microphysical and radiative properties of cirrus clouds to climate and climatic feedback. *J. Atmos. Sci.,* **47,** 1742–1753.

Takahashi, T., and N. Fukuta, 1988: Supercooled cloud tunnel studies on the growth of snow crystals between −4 and −20°C. *J. Meteor. Soc. Japan,* **66,** 841–855.

——, T. Endoh, G. Wakahama, and N. Fukuta, 1991: Vapor diffusional growth of free-falling snow crystals between −3 and −23°C. *J. Meteor. Soc. Japan,* **69,** 15–30.

Todd, C. J., 1965: Ice crystal development in a seeded cumulus cloud. *J. Atmos. Sci.,* **32,** 70–78.

Weickmann, H., 1949: Des Eisphase in der Atmosphäre. *Ber. Dtsch. Wetterdienstes U.S. Zone,* **6,** 54.

Wielicki, B. A., J. T. Suttles, A. J. Heymsfield, R. M. Welch, J. D. Spinhirne, M. L. Wu, D. O'C. Starr, L. Parker, and R. F. Arduini, 1990: The 27–28 October 1986 FIRE IFO cirrus case study: Comparison of radiative transfer theory with observations by satellite and aircraft. *Mon. Wea. Rev.,* **118,** 2356–2370.